Journal of Molecular Modeling (2019) 25: 61
https://doi.org/10.1007/s00894-019-3942-6

ORIGINAL PAPER

Exploring the mechanism of alkene hydrogenation catalyzed by defined iron complex from DFT computation

Cai-Hong Guo[1] · Dandan Yang[1] · Xiaoyan Liu[1] · Xiang Zhang[1] · Haijun Jiao[2]

Received: 3 October 2018 / Accepted: 24 January 2019 / Published online: 12 February 2019

Abstract

UB3LYP computation including dispersion and toluene solvation has been carried to elucidate the mechanisms of alkene hydrogenation catalyzed by bis(imino)pyridine iron dinitrogen complex (^{iPr}PDI)Fe(N_2)$_2$, which has low stability towards N_2 dissociation. The coordinatively unsaturated complexes, (^{iPr}PDI)Fe(N_2) and (^{iPr}PDI)Fe(1-C_4H_8), favor open-shell singlet ground states. On the basis of our computations, we propose a new mechanism of 1-butene coordination and hydrogenation after N_2 dissociation. The hydrogenation of 1-butene undergoes a concerted open-shell singlet transition state involving H_2 dissociation, C-H bond formation and C=C bond elongation, as well as the subsequent C-H reductive elimination. In the whole alkene hydrogenation, the H-H bond cleavage is the rate-determining step.

Keywords Alkene hydrogenation · Fe complexes · DFT · Mechanism · Homogeneous catalysis

Introduction

Hydrogenation of alkenes catalyzed by homogeneous transition metal compounds is one of the widely studied reactions in modern chemistry [1]. This powerful transformation has been widely applied in commercial processes for pharmaceutical, fine, and commodity chemical synthesis [2–6]. Since the discovery of the Wilkinson catalyst (Ph_3P)$_3$RhCl over half a century ago [7, 8], the most commonly employed protocols involve the use of catalysts based on precious metals like rhodium, iridium, and ruthenium [9–13]. Alternatively, earth-abundant base iron catalysts have been developed by several laboratories during the past few decades [14, 15].

One interesting type of hydrogenation catalysts is the aryl-substituted bis(imino)pyridine transition metal (PDI)M complexes [PDI = 2,6-(R^1N=CR^2)$_2$$C_5H_3N$; R^1 = alkyl, aryl, amino; R^2 = H, Me]. Initial studies by Brookhart and Gibson revealed that Co(II) and Fe(II) complexes containing (imino)pyridine ligands with bulky aryl substituents at the imine position are highly active and long-lived for ethylene polymerization [16, 17]. Among different hydrogenation catalysts, cobalt and rhodium bis(imino)pyridine complexes have been utilized for the hydrogenation of mono- and disubstituted olefins [18].

The first bis(imino)pyridine iron bis(dinitrogen) complex (^{iPr}PDI)Fe(N_2)$_2$ [^{iPr}PDI = (2,6-(2,6-^{i}Pr$_2$-C_6H_3N=CMe)$_2$$C_5H_3N$)] (Scheme 1) was reported by Chirik et al. [19] They found that (^{iPr}PDI)Fe(N_2)$_2$ is an effective pre-catalyst for olefin hydrogenation, like 1-hexene, under ambient temperature and one atmosphere H_2 pressure with high turnover frequencies. Later, Chirik et al. [20], prepared the phenyl-substituted bis(imino)pyridine iron bis(dinitrogen) complex (^{iPr}PhPDI)Fe(N_2)$_2$ [^{iPr}PhPDI = 2,6-(2,6-^{i}Pr$_2$-C_6H_3N=CPh)$_2$$C_5H_3N$] and demonstrated that this phenyl-substituted catalyst (^{iPr}PhPDI)Fe(N_2)$_2$ is more productive than (^{iPr}PDI)Fe(N_2)$_2$ for 1-hexene hydrogenation, but inferior for the traditionally more hindered substrates like cyclohexene and (+)-(*R*)-limonene. In addition, complex (^{iPr}PDI)Fe(N_2)$_2$

Dedicated to Prof. Dr. Tim Clark on the occasion of his 70th birthday

This paper belongs to the Topical Collection Tim Clark 70th Birthday Festschrift

Electronic supplementary material The online version of this article (https://doi.org/10.1007/s00894-019-3942-6) contains supplementary material, which is available to authorized users.

✉ Cai-Hong Guo
sxgch2006@163.com

✉ Haijun Jiao
haijun.jiao@catalysis.de

[1] Key Laboratory of Magnetic Molecules, Magnetic Information Materials Ministry of Education, The School of Chemical and Material Science, Shanxi Normal University, Linfen 041004, China

[2] Leibniz-Institut für Katalyse e.V. an der Universität Rostock, Albert-Einstein-Strasse 29a, 18059 Rostock, Germany

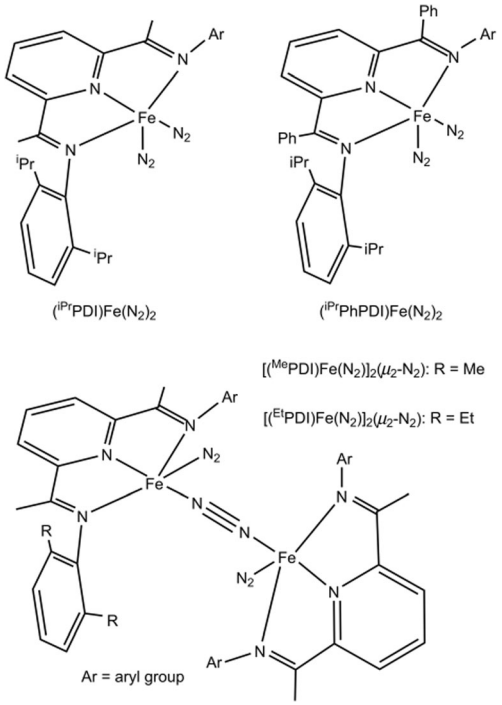

Scheme 1 Bis(imino)pyridine iron dinitrogen complexes used for alkene hydrogenation by Chirik et al.

can be used for the hydrogenation of aryl azides to the corresponding anilines [21]. The catalytic performance of (^{iPr}PDI)Fe(N_2)$_2$ on the hydrogenation of a range of substituted alkenes, such as amino- and oxygen-substituted alkenes, have been explored by Chirik et al. [22] The new dimeric, aryl-substituted bis(imino)pyridine iron dinitrogen complexes were synthesized and characterized [23, 24]. Compared with the original complex (^{iPr}PDI)Fe(N_2)$_2$, complex [(^{Me}PDI)Fe(N_2)]$_2$(μ_2-N_2) offers dramatically improved activity for the hydrogenation of ethyl-3-methylbut-2-enoate [23, 24]. Despite the exploration of iron catalysts with the redox-active bis(imino)pyridine ligand or the weak-field ligand, the catalytic reaction pathways still remain unclear due to the short lifetime of catalyst and intermediates. Redox-active ligands may occur in several different formal oxidation states when bound to the first row transition metals [25]. The spin state crossing ("two-state reactivity") is necessary when there are different spin states in catalysts and intermediates [26]. When spin-orbit coupling is sufficient to allow the molecule(s) to traverse between the potential energy surfaces (PES) within a reaction, spin state changes can occur [27]. A recent report shows that bis(imino)pyridine iron alkyl complexes have a high-spin iron(II) center, which is antiferromagnetically coupled to chelate radical anions [28].

Although previous work proposed a plausible mechanism (Scheme 2) [19], the detailed kinetic information and crucial intermediates were unclear. It is proposed that the initial step is the generation of the active catalyst via N_2 dissociation, following by 1-butene coordination. In path **I**, direct H_2 oxidative

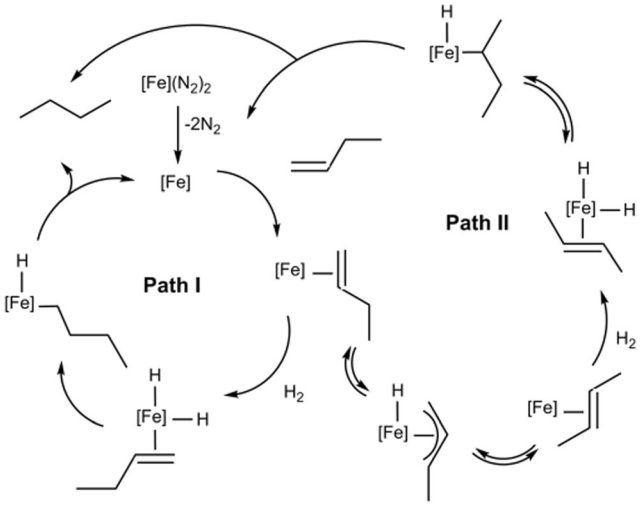

Scheme 2 Proposed mechanism of butene hydrogenation with [Fe](N_2)$_2$, [Fe] = (^{iPr}PDI)Fe [19]

addition to the Fe center of (^{iPr}PDI)Fe(CH_2 = $CHCH_2CH_3$) leads to iron(II) dihydride complex (^{iPr}PDI)Fe(H)$_2$(CH_2 = $CHCH_2CH_3$) and the next step is the stepwise transfer of hydride ligand to 1-butene and butyl ligands. In path **II**, the isomerization of 1-butene catalyzed by (^{iPr}PDI)Fe takes place to form 2-butene-coordinated iron complex and the next step is the stepwise transfer of hydride ligand to 2-butene and 2-butyl ligands. To elucidate the alkene hydrogenation mechanism catalyzed by (^{iPr}PDI)Fe(N_2)$_2$, we carried out detailed density functional theory calculations. Possible reaction paths including closed-shell singlet, open-shell singlet, and open-shell triplet states were investigated comprehensively, in order to identify different pathways of H_2 oxidative addition and obtain the insights into the reaction mechanism of olefin hydrogenation. These insights should be helpful for the understanding into the catalytic activity of low-oxidation-state iron complexes.

Computational details

Geometry optimizations were performed at the level of UB3LYP density functional theory [29–31], which was adopted in previous works on the detailed mechanisms of alkene polymerization and oligomerization process initiated by bis(imino)pyridyl-iron catalysts [32] and N-H insertion reactivity of iron porphyrin carbene [33]. We used the real (^{iPr}PDI)Fe(N_2)$_2$ complex without any simplifications as pre-catalysts and 1-butene as substrate. The validity of our treatment has been established in the previous study of similar systems and it is not expected to affect the mechanistic results [34, 35]. The iron atom was performed with the effective core potential based LANL2DZ basis set [36] and the 6-31G(d) basis set was used for all other atoms [37, 38]. This basis set is denoted as BSI. The harmonic vibrational frequencies were

calculated at the same level to characterize the nature of the stationary points as true minima without imaginary frequencies or authentic transition states with only one imaginary frequency. Especially, the validity of transition states was confirmed by intrinsic reaction coordinate (IRC) computation and the connectivity between stationary points was established [39, 40]. All complexes in the open-shell singlet were calculated by using the symmetry-broken method as used in previous studies [41–43]. Natural bond orbital (NBO) analysis has been explored to provide natural population analysis (NPA) charges [44].

To confirm the reliability of the chosen theory level, we made specific search on geometry optimization and energy computations (Fig. S1). The computed bond distances of (^{iPr}PDI)Fe(N_2)$_2$ at B3LYP/BSI and B3LYP/BSII (BSII denotes the combination of LANL2DZ for Fe and 6–31 + G(d,p) for other atoms) differ very slightly (Table S1), and they are in good agreement (> 97%) with the available data from X-ray structure diffraction analysis (Table S2). To save computing costs, we used B3LYP/BSI to optimize the structures of all intermediates and transition states at first and then refined the energies with B3LYP/6–311++G(d,p)//B3LYP/BSI and B3LYP-D3/6–311++G(d,p)//B3LYP/BSI single-point energy calculations with solvent effects accounted by the conductor-like polarizable continuum model (CPCM) [45] and polarizable continuum model (PCM) [46, 47]. The dielectric constant (ε) of the polarizable medium toluene was set to 2.379, which was the solvent used in related experiments. The final B3LYP-D3 (with PCM)/6–311++G(d,p)//B3LYP/BSI electronic energies were added to the Gibbs free energy correction calculated at B3LYP/BSI level to obtain the final presenting Gibbs free energy in solution. The functional B3LYP-D3 shows good performance due to its inclusion of dispersion effects [48, 49]. In addition, we have compared M06 and B3LYP functional (Table S5) to reevaluate the relative energy and found that for **3a** the single-point M06/6–311++G(d,p) or M06-2X/6–311++G(d,p) energies including dispersion and toluene solvation are close to that B3LYP-D3; and for the dissociation of N2 from (^{iPr}PDI)Fe(N_2)$_2$, the B3LYP-D3 method is best (Table S4). Although the thermal and entropy contributions to the Gibbs free energy were incorporated from the gas phase frequency calculations at 1 atm pressure and 298 K, the entropy contribution was overestimated from the gas-phase calculations, especially for the cases where the numbers of reactant and product molecules are different, i.e., correction is added to the free energies according to the free volume theory. For one-to-one or two-to-two transformation, no correction was made. For two-to-one (or one-to-two) transformation, a correction of − 1.89 (or 1.89) kcal/mol was made at the temperature of 298.15 K [50].

In the reaction pathways, the species with OS denotes the open-shell singlet, such as ^{OS}**2a**, and the 3 denotes the triplet state, such as ^{3}**2a**. The "guess = alter" keyword was employed to obtain the open-shell singlet electronic structures. The wave function stability has been performed on all open-shell singlets by using a "stable = opt" calculation [51, 52]. The wave function of all open-shell singlets is stable and the <S2> values have been given in Table S6 to show the spin contaminations. Table S6 shows the energy changes upon Yamaguchi correction [53] for the open-shell singlet species. The correction stabilizes the open-shell singlet species, but the annihilation of the spin contamination is incomplete in these species. In order to consider all possible open-shell singlet solutions, a spin-unrestricted broken-symmetry (BS) model was investigated using the fragment guess feature. In the BS calculations, we defined three fragments for all species; Fe/Fe-H, PDI, and N_2/C_4H_8. In BS(m,n) formulation, m is the number of electrons on the Fe center, and n is the number of electrons on the PDI fragment; and both types of electrons couple in an antiferromagnetic way. Two different BS approaches, BS(1,1) corresponding to the antiferromagnetic coupling between Fe^{I} (d^7, S_{Fe} = 1/2) and the PDI doublet anion ligand (PDI^{-}, S_{PDI} = 1/2) as well as BS(2,2) corresponding to the antiferromagnetic coupling between Fe^{II} (d^6, S_{Fe} = 1) and PDI triplet dianion ligand (PDI^{2-}, S_{PDI} = 1), were carried. It is found that both BS approaches converged to the one solution, which is the same as obtained using "guess = alter". It is noted that most of the open-shell singlets have the same energy by using two methods except for ^{OS}**5a** and ^{OS}**5b**. The relative energies of ^{OS}**5a** and ^{OS}**5b** using "guess = fragment" are slightly lower than those using "guess = alter" (− 8.80 vs. − 12.11 kcal/mol; and − 10.00 vs. −13.97 kcal/mol before Yamaguchi correction, respectively). All calculations were performed with the Gaussian 09 software package [54].

Results and discussion

Catalyst activation as well as H_2 and 1-butene coordination

The optimized molecular structure of the real catalyst (^{ipr}PDI)Fe(N_2)$_2$ [**1-(N_2)$_2$**] in singlet state has a distorted square pyramid with one N_2 ligand completing the fourth site of the basal plane, while the other N_2 ligand occupies the apical position. This is in full agreement with the single crystal structure of **1-(N_2)$_2$** [19]. Similar to the previous suggested electron structure for **1-(N_2)$_2$**, the BS(1,1) solution is 2.63 [11.66] kcal/mol more stable than the closed-shell singlet [55]. Attempts to optimize the triplet and quintet states of **1-(N_2)$_2$** led to the dissociation of one N_2 ligand, indicating the instability of **1-(N_2)$_2$** in high spin states. The obvious difference between the susceptibility of the open-shell singlet and that of the closed-shell singlet is that a closed-shell singlet is usually diamagnetic, except when the temperature-independent

paramagnetic interactions with relatively high energy excited states are strong enough, whereas the open-shell singlet is a temperature-independent paramagnet [56]. For the open-shell singlet, the spin is zero, but the orbital angular momentum is not. Therefore, the calculated open-shell singlet electronic structure for **1-(N$_2$)$_2$** is antiferromagnetic, which is consistent with the paramagnetic **1-(N$_2$)$_2$** in solid state examined by the SQUID data from 4 to 300 K [19]. Our calculations show that ^{OS}**1-(N$_2$)$_2$** has spin density at Fe (ρ = 0.954) and the PDI fragment (ρ = − 0.858). The NMR spectroscopy of **1-(N$_2$)$_2$** shows the dynamic coordination and dissociation of N_2 ligand from **1-(N$_2$)$_2$** [19]. We looked back to the SQUID data for **1-(N$_2$)$_2$** in the original paper of Chirik [19]. We analyzed the χT-T figure and endued that the paramagnetism in the high temperature region (above circa 30 K) is originated from **1-N$_2$** and the antiferromagnetism in the low temperature region is originated from **1-(N$_2$)$_2$**. The Weiss constant (θ) fitted out with Curie-Weiss law has a small negative value of − 0.64(2), which ruled out the diamagnetic behavior in the low-temperature region. Based on our calculations, **1-(N$_2$)$_2$** has an open-shell singlet ground state, which verified the antiferromagnetism in the low temperature. Therefore, the description of the diamagnetic ground state of **1-(N$_2$)$_2$** in the later paper of Chirik is probably not correct [55].

Prior to catalysis, the pre-catalyst needs to discard one or two N_2 ligands to form the coordinatively unsaturated and active species; (^{ipr}PDI)Fe(N_2) [**1-N$_2$**] or (^{ipr}PDI)Fe [**1**]. Experimentally, it is found that (^{iPr}PDI)Fe(N_2)$_2$ in toluene undergoes N_2 dissociation and forms equilibrium between (^{iPr}PDI)Fe(N_2)$_2$ and (^{iPr}PDI)Fe(N_2), in favor of (^{iPr}PDI)Fe(N_2). The dissociation of the first N_2 ligand from **1-(N$_2$)$_2$** into the singlet state (**1-N$_2$**) is endergonic by 14.04 kcal/mol, while exergonic into the triplet state (^{3}**1-N$_2$**) by 2.08 kcal/mol and the open-shell singlet state (^{OS}**1-N$_2$**) by 3.71 [5.80] kcal/mol (Fig. 1), indicating the low thermodynamic stability of **1-(N$_2$)$_2$** as well as the preference of (^{iPr}PDI)Fe(N_2) as well as the possible equilibrium between (^{iPr}PDI)Fe(N_2)$_2$ and (^{iPr}PDI)Fe(N_2).

On the potential energy surface, ^{3}**1-N$_2$** and ^{OS}**1-N$_2$** are much more stable than **1-N$_2$** by 16.12 and 17.73 [19.82] kcal/mol at ambient temperature (298.15 K), close to 16.0 kcal/mol reported by the Chirik's group [55]. Such energetic changes also have been found by using different methods (Tables S3 and S4). The scene of spin-forbidden ligand dissociation is very common in organometallics [57–59]. To afford ^{3}**1-N$_2$** the spin-change should take place. As shown in Fig. 2, ^{3}**1-N$_2$** involves spin density at Fe(I) (ρ = 1.238) and PDI$^-$ (ρ = 0.779); and ^{OS}**1-N$_2$** has spin density at

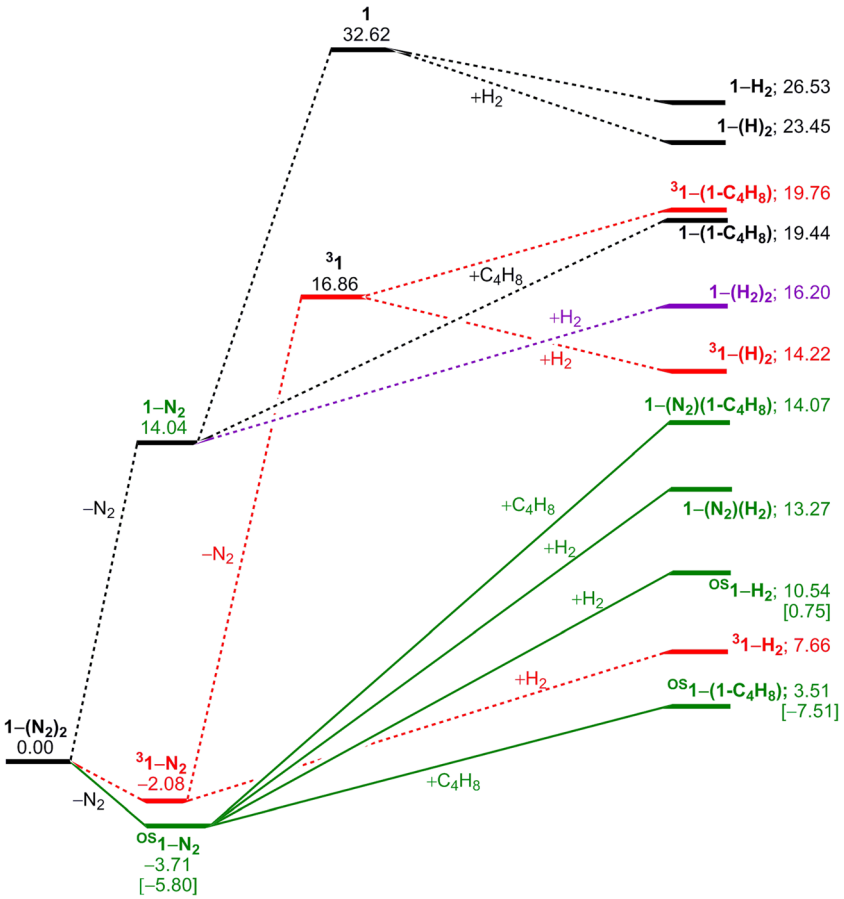

Fig. 1 Free energies (Δ*G*, kcal/mol) for N_2 dissociation from (^{iPr}PDI)Fe(N_2)$_2$, followed by H_2 or 1-butene coordination/replacement. The Yamaguchi correction for the open-shell singlet species is given in *square brackets*

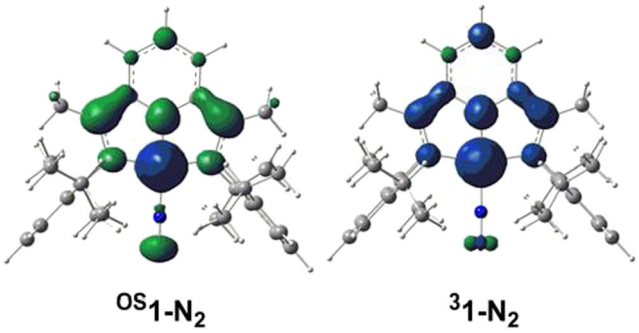

Fig. 2 Spin densities of the open-shell singlet ^{OS}1-N_2 and triplet ^{3}1-N_2

Fe (ρ = 1.358) and the PDI fragment (ρ = − 1.182). This indicates the contribution of antiferromagnetic coupling between Fe(II) and a diradical dianion PDI^{2-}, in agreement with the study on the multireference electronic structure of (PDI)FeN_2 [60]. The calculated stability of ^{OS}**1-N_2** is in line with that of the (^{iPr}EtPDI)FeN_2 and (^{iPr}iPrPDI)FeN_2 complexes [55]. The recent multireference study on the different spin states of the PDI-ligated Fe complexes show that the BS(4,2) septet, BS(3,1) quintet, and BS(3,1) triplet states with ρ(Fe) > 3 are not only higher in energy than the triplet and open-shell singlet BS(1,1) but also have the Fe–N bond distance significantly longer than the experimentally determined value [60]. Thus, we did not further consider the high spin states on the Fe center.

Without alkene or H_2 coordination, the dissociation of the second N_2 ligand from ^{3}**1-N_2**/^{OS}**1-N_2** into the triplet state ^{3}**1** or the singlet **1** is endergonic by 18.94/20.57 [22.66] or 34.70/36.33 [38.42] kcal/mol, respectively, indicating the high thermodynamic stability of ^{3}**1-N_2** and ^{OS}**1-N_2**. The open-shell singlet for **1** cannot be obtained. Furthermore, we computed the coordination of H_2 and 1-butene (1-C_4H_8) to ^{3}**1-N_2** and ^{OS}**1-N_2**. Our results show that 1-butene coordination to ^{3}**1-N_2**/^{OS}**1-N_2** to form **1-(N_2)(1-C_4H_8)** is endergonic by 16.15/17.78 [19.87] kcal/mol and H_2 coordination to ^{3}**1-N_2**/^{OS}**1-N_2** to form **1-(N_2)(H_2)** is endergonic by 15.35/16.98 [19.07] kcal/mol.

To show the participation of substrates in promoting the activation of ^{3}**1-N_2** and ^{OS}**1-N_2**, we computed the substitution of N_2 in ^{3}**1-N_2**/^{OS}**1-N_2** by H_2 and 1-butene (1-C_4H_8). The substitution of N_2 in ^{3}**1-N_2**/^{OS}**1-N_2** by 1-butene to form the singlet state **1-(1-C_4H_8)**, triplet state ^{3}**1-(1-C_4H_8)** and open-shell singlet state ^{OS}**1-(1-C_4H_8)** is endergonic by 21.52/23.15 [25.24], 21.84/23.47 [25.56], and 5.59/7.22 [−5.43/−1.71] kcal/mol, respectively, indicating that 1-butene prefers N_2 substitution to form the open-shell singlet state ^{OS}**1-(1-C_4H_8)** rather than the coordination to form the singlet **1-(N_2)(1-C_4H_8)**. The substitution of N_2 in ^{3}**1-N_2**/^{OS}**1-N_2** by H_2 to form the singlet state **1-H_2**, triplet state ^{3}**1-H_2** and the open-shell singlet state ^{OS}**1-H_2** is endergonic by 28.61/30.24 [32.33], 9.74/11.37 [13.46], and 12.62/14.25 [2.83/6.55] kcal/mol, respectively, indicating that H_2 prefers N_2 substitution to form the triplet state ^{3}**1-H_2** (the open shell singlet ^{OS}**1-H_2** after Yamaguchi correction) rather than coordination to form the singlet **1-(N_2)(H_2)**. It also shows that N_2 substitution by 1-butene to form the open-shell singlet state ^{OS}**1-(1-C_4H_8)** is more favored than N_2 substitution by H_2 to form the triplet state ^{3}**1-H_2** by 4.15 [15.17] kcal/mol and to form ^{OS}**1-H_2** by 7.03 [8.26] kcal/mol.

In the geometry of ^{3}**1-H_2**, the H_2 ligand coordinates to the Fe center in η^2 fashion vertically with respect to N-Fe-N plane and forms a distorted square planar coordination sphere, where the H_2 ligand has molecular coordination as indicated by the H-H distance of 0.825 Å, which is slightly elongated as compared with free H_2 molecule (0.743 Å). In **1-H_2**, the H_2 ligand lies on the equatorial plane of N-Fe-N. Thermodynamically, ^{3}**1-H_2** is more stable than **1-H_2** and ^{OS}**1-H_2** by 18.87 and 2.88 kcal/mol (^{OS}**1-H_2** is more stable than **1-H_2** and ^{3}**1-H_2** by 25.78 and 6.91 kcal/mol after Yamaguchi correction), respectively. In addition, the dihydride complexes ^{3}**1-(H)$_2$** and **1-(H)$_2$** from H_2 oxidative addition are less stable than ^{3}**1-H_2** by 6.56 and 15.79 kcal/mol (less stable than ^{OS}**1-H_2** by 13.47 and 22.70 kcal/mol after Yamaguchi correction), respectively. All these indicate that the stable intermediates ^{3}**1-N_2** and ^{OS}**1-N_2** are afforded at the initial stage of reaction and the next step should be 1-butene substitution with the formation of open-shell singlet state ^{OS}**1-(1-C_4H_8)** in the environment of 1-butene and H_2. This supports the reaction intermediate (^{iPr}PDI)Fe(CH_2 = $CHCH_2CH_3$) suggested by Chirik and coworkers [19].

1-Butene hydrogenation

Considering that the spin state pre-equilibrium is established between ^{OS}**1-N_2** and ^{3}**1-N_2** due to the small energy difference (1.63 [3.72] kcal/mol), we computed the open- and closed-shell singlet states as well as triplet states for all intermediates and transition states. As shown in Fig. 3 and Fig. S2, the open-shell singlet ^{OS}**1-(1-C_4H_8)** exhibits anti-ferromagnetic coupling between the unpaired d-electron of Fe (ρ = 1.596) and the PDI fragment (ρ = − 1.417), with a charge distribution as Fe(+I)-$(PDI)^{1-}$. The triplet ^{3}**1-(1-C_4H_8)** involves a high-spin Fe(I) (ρ = 1.260) and PDI^{-} (ρ = 0.849).

Firstly, H_2 coordination to ^{OS}**1-(1-C_4H_8)** forms the open-shell singlet complex [Fe](H_2)(1-C_4H_8) (^{OS}**2**) in distorted square pyramid coordination sphere. There are two possible conformers, one with the C_2 carbon close to H_2 ligand (^{OS}**2a**); and one with C_1 carbon close to H_2 (^{OS}**2b**). As expected, H_2 coordination to ^{OS}**1-(1-C_4H_8)** to form ^{OS}**2a** and ^{OS}**2b** is endergonic by 11.50 [17.03] and 13.46 [18.84] kcal/mol. The closed-shell singlet and triplet states are higher in energy than the open-shell singlet state (Fig. 4 and Fig. S3). It is noted that only molecular coordinated H_2 complexes are found in ^{OS}**2a**/**2a** and ^{OS}**2b**/**2b**; and it is not possible to find any dissociatively coordinated dihydride complexes from the

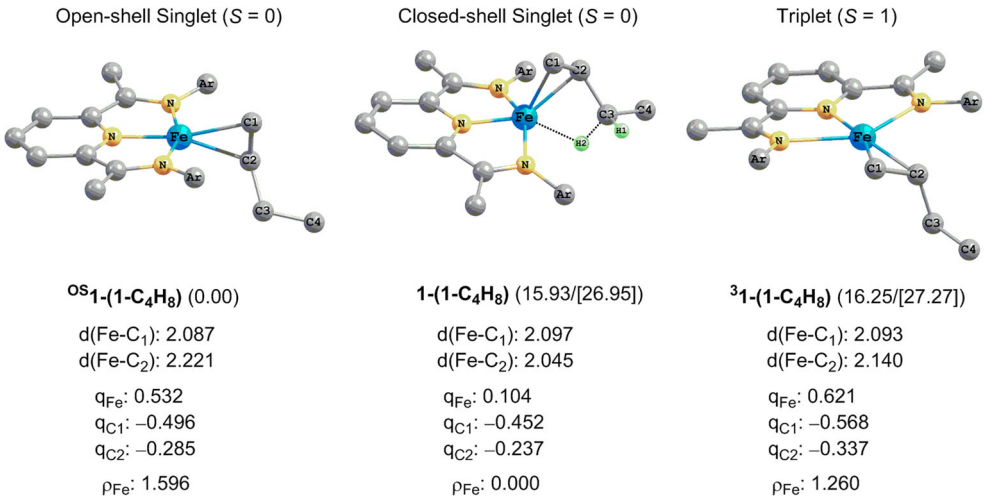

Fig. 3 Free energies (ΔG, kcal/mol) of complex 1-(1-C_4H_8) including geometric parameters, NBO charges (q) and Mulliken spin densities of iron. The Yamaguchi correction for the open-shell singlet species is given in *square brackets*

directly oxidative addition, different from the proposed iron(II) dihydride complex $(CH_2=CHCH_2CH_3)[Fe](H)_2$ by Chirik et al. [19]. Previous experiments showed that the pyridine bis(phosphine) iron(II) dihydride complexes were prepared from hydride addition [61, 62]. The electron-withdrawing redox-active bis(imino)pyridine disfavors H_2 direct oxidative addition H_2 to iron(0), while the electron-donating pyridine bis(carbene) ligand enables H_2 oxidative addition to iron(0) [63].

From complex ^{OS}**2a**, we computed 1-butene hydrogenation (Fig. 4). At first, we located the open-shell singlet transition state [^{OS}**TS(2a/3a)**] for 1-butyl formation with hydrogen attacking the C_2 carbon, i.e.; a transition state for H-H dissociation (1.120 Å) and C–H bond formation (1.543 Å) as well as C=C double bond elongation (1.434 Å). Since H_2 coordination and H-H bond cleavage take place concurrently, ^{OS}**TS(2a/3a)** is a multi-bond concerted transition state [64]. For comparison, we further optimized **2a**, **TS(2a/3a)**, and **3a**

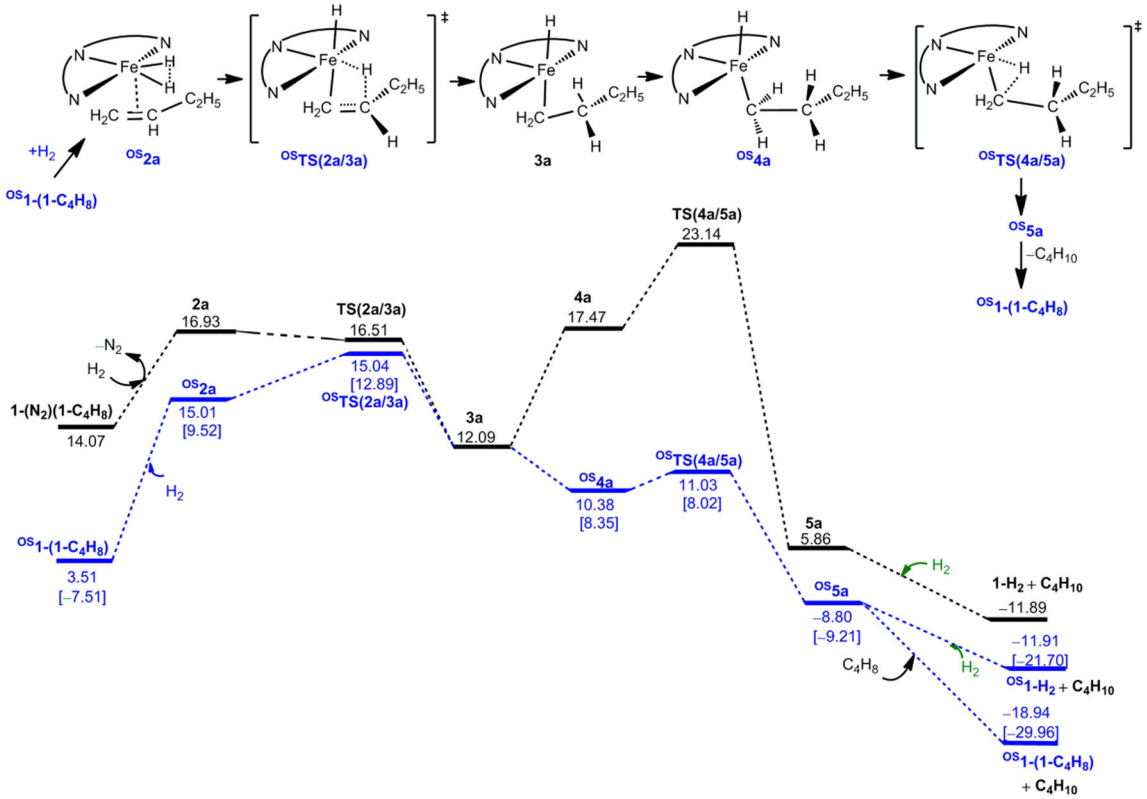

Fig. 4 Free energy profiles (ΔG, kcal/mol) along the path with H_2 coordination and 1-butene hydrogenation (the *black lines* are for closed-shell singlet states; the *blue lines* are for open-shell singlet states). The Yamaguchi correction for the open-shell singlet species is given in *square brackets*

in toluene and found that structural parameters of these species in gas phase and toluene are almost the same.

The hydrogenation of 1-butene affords 1-butyl complex **3a**, in which the 1-butyl ligand agostically interacts with the Fe center. In **3a**, the Fe···H–C agostic bond is 1.810 Å, and the C=C double bond is elongated to 1.498 Å as well as the dissociated H–H distance is 1.925 Å. We searched for the open-shell singlet state for **3a**, but it collapsed to the closed-shell singlet. Starting from complex ^{OS}**2a**, 1-butene hydrogenation affording 1-butyl complex **3a** is exergonic by 2.92 kcal/mol (however, it is endergonic by 3.57 kcal/mol after Yamaguchi correction), and the associated barrier is only 0.03 [3.37] kcal/mol, indicating that the σ-bond metathesis between the bound H_2 and 1-butene takes place easily. This is similar to the fact that the σ-bond metathesis between the bound H_2 and Ir-ethyl moiety overcomes relatively low energetic span in the iridium-catalyzed alkene hydrogenation [65], and iron dialkyl complexes have been reported [66, 67]. Noticeably, the closed-shell singlet [**TS(2a/3a)**] and triplet state [^{3}**TS(2a/3a)**] transition states are 1.47 [3.62] and 16.74 [18.89] kcal/mol above the open-shell singlet transition state ^{OS}**TS(2a/3a)**, respectively. The triplet 1-butyl complex ^{3}**3a** is less stable than **3a** by 17.24 kcal/mol. On the basis of our calculations, the C=C bond activation and hydrogenation occurs through the open-shell singlet state path, and the overall barrier is 15.04 [12.89] kcal/mol.

After **3a**, the C–H reductive elimination was considered. Since H_1 and C_1 atoms in **3a** are on different sides of the N-Fe-N plane, the H_1 atom cannot attack the C_1 atom directly; and therefore 1-butyl rotation is indispensable. However, attempts to locate a transition state for 1-butyl clockwise rotation around the Fe–$N_{pyridine}$ axis failed. On the basis of the rotated 1-butyl ligand, we located species **4a**, which is less stable than **3a** by 5.38 kcal/mol. It is worth noting that a potential energy surface scan from **3a** is uphill, indicating that no transition state exists. Interestingly, the open-shell singlet ^{OS}**4a** and the triplet state ^{3}**4a** are more stable than its singlet **4a** by 7.09 [9.12] and 12.99 kcal/mol. We also located the authentic triplet three-center transition state ^{3}**TS(4a/5a)** between ^{3}**4a** and ^{3}**5a**. Compared with the close-shell singlet transition state **TS(4a/5a)** and the triplet transition state ^{3}**TS(4a/5a)**, the open-shell singlet transition state ^{OS}**TS(4a/5a)** has the lowest energy, indicating that the C-H reductive elimination occurs via the open-shell singlet state path with low barrier of 0.65 kcal/mol. From **3a**, the open-shell singlet state is below the triplet and closed-shell singlet states. Here, the 1-butyl hydrogenation from **4a** proceeds via the open-shell singlet pathway, which is different in the styryl ligand hydrogenation catalyzed by triplet (TPB)Fe(μ-H)(H) [68]. Based on the singlet and the triplet potential energy surfaces (PES), from **3a**, the weaker 1-butyl ligand dissociation or rotation features no spin acceleration [69]. Finally, one molecular C_4H_8 enters the coordinate site of iron and the 1-butane releases. The geometries of the closed-shell singlet intermediates and transition states are displayed in Fig. S4.

We investigated another alkene hydrogenation but it needs overcoming relatively higher barrier (Fig. S5 and S6). Starting from the less stable ^{OS}**2b**, we computed the transition state **TS(2b/3b)** for 2-butyl formation with hydrogen attacking the C_1 carbon, and the barrier is 18.23 [29.25] kcal/mol, higher than that of 1-butyl formation (11.53 [20.40] kcal/mol). In addition, **3a** is more stable than **3b** by 8.83 kcal/mol. This indicates that **3a** formation is more favored kinetically and thermodynamically than **3b** formation. Nevertheless, we computed the subsequent reaction for **3b**. The difference is that three states for **3b** almost have the same high energy and the same geometric feature. From **3b**, the triplet states lie below the closed- and open-shell singlet states (the open-shell singlet states ^{OS}**TS(4b/5b)** and ^{OS}**5b** lie below the corresponding closed- and triplet states after Yamaguchi correction). The C-H reductive elimination takes place via ^{3}**TS(4b/5b)** with an moderate barrier of 10.60 kcal/mol (via ^{OS}**TS(4b/5b)** with an moderate barrier of 6.66 [1.73] kcal/mol after Yamaguchi correction), which is higher than that (0.65 kcal/mol) along the path initiated by species ^{OS}**4a**. Thus, the path along with **2a** is more favorable than the path along with **2b**. All computational details are listed in the Supplementary material for comparison.

Previous studies on the Pt- and Rh-catalyzed hydrosilylation of alkenes show that ethylene coordination with the Pt(II) or Rh(II) center can lower the barrier of Si–C or C–H reductive elimination [70–72]. Thus, we explored H_2 or N_2-promoted C–H reductive elimination (Fig. S7). It was found that the coordination of one molecular N_2 or H_2 to the Fe center of **3a** by breaking the agostic interaction is endergonic by 8.97 or 13.25 kcal/mol, respectively; and the subsequently promoted transition state for C–H reductive elimination is higher than that of ^{OS}**TS(4a/5a)** by 9.70 [12.71] and 15.38 [18.39] kcal/mol, respectively. Such energy increase rules out the promotion effect for additional N_2 and H_2 coordination, different from the fact that the oxidative cleavage of the H_2 to form Ir–H bond occurs before the C–H reductive elimination [73].

1-Butene isomerization and H_2 addition

Since N_2 substitution by 1-butene to form the open-shell singlet state ^{OS}**1-(1-C_4H_8)** is more favored than N_2 substitution by H_2 to form the triplet state ^{3}**1-H_2** by 4.15 kcal/mol (to form the open-shell singlet state ^{OS}**1-H_2** by 8.26 kcal/mol after Yamaguchi correction), we computed the potential energy surface according to the proposed isomerization and hydrogenation path for comparison (Fig. 5 and Fig. S8). Due to the planar geometry of **1-N_2**/^{OS}**1-N_2**, the incoming 1-butene may attack the axial site to form **1-(N_2)(1-C_4H_8)** or directly replace the N_2 ligand to form **1-(1-C_4H_8)**; and the former is

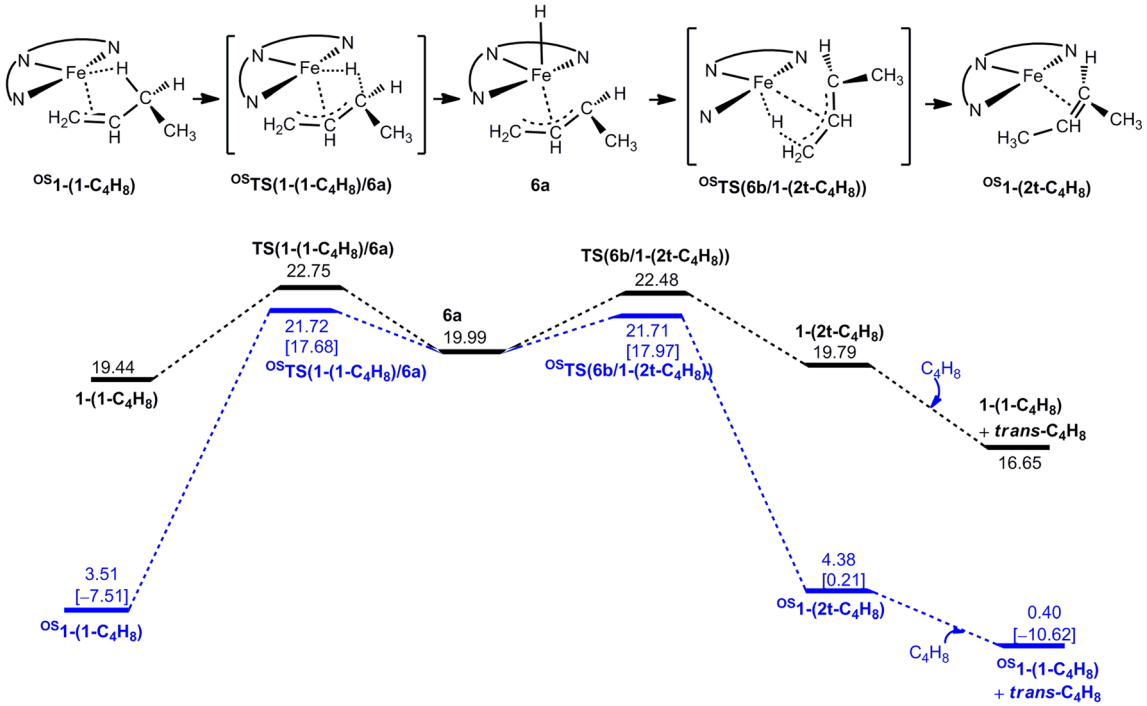

Fig. 5 Free energy profiles (ΔG, kcal/mol) along the path with 1-butene isomerization and hydrogenation (the *black line* is for closed-shell singlet; the *blue line* for open-shell singlet). The Yamaguchi correction for the open-shell singlet species is given in *square brackets*

found endergonic by 17.78 [19.87] kcal/mol, while the latter is found endergonic by 7.22 kcal/mol (exoergic by 1.71 kcal/mol after Yamaguchi correction) to form ^{OS}**1-(1-C$_4$H$_8$)** and endergonic by 23.15 [25.24] kcal/mol to form **1-(1-C$_4$H$_8$)**. Obviously, the reaction undergoes the replacement of N_2 in ^{OS}**1-N$_2$** by 1-butene to form ^{OS}**1-(1-C$_4$H$_8$)**. The Fe···H–C agostic interaction in **1-(1-C$_4$H$_8$)** (Fe···H-C distance is 1.880 Å) enables the C-H bond activation and the subsequent isomerization, as reported in the bifunctional ruthenium-catalyzed alkene isomerization via similar agostic Ru···H–C intermediate [74]. Moreover, we found that the geometry of ^{OS}**1-(1-C$_4$H$_8$)** is also in favor of 1-butene isomerization. Complex ^{OS}**1-(1-C$_4$H$_8$)** dominates the reaction due to its relatively high stability over **1-(1-C$_4$H$_8$)**.

From **1-(1-C$_4$H$_8$)**, the shift of the agostic H_1 to the Fe center, leading to the η^3-allyl hydride species (η^3-C_4H_7)[Fe]H (**6a**), takes place via the authentic transition state **TS(1-(1-C$_4$H$_8$)/6a)**. This scene appeared in the olefin isomerization reaction [74]. One can see that the Fe–H_1 bond in **TS(1-(1-C$_4$H$_8$)/6a)** is obviously shortened (1.556 Å) with respect to the length of Fe···HC agostic value (1.880 Å). The imaginary frequency of **TS(1-(1-C$_4$H$_8$)/6a)** displays the desired displacement orientation. Similar η^3-allyl intermediates have also been found in other iron carbonyl [75, 76] and palladium-catalyzed [77, 78] alkene isomerization reactions. This transformation process (**1-(1-C$_4$H$_8$)** → **6a**) has a barrier of 3.31 kcal/mol, lower than that (8.7 kcal/mol) catalyzed by $Fe(CO)_3$ fragment [79]. The conversion of **1-(1-C$_4$H$_8$)** to **6a** is predicted to be endergonic by 0.55 kcal/mol. For the isomerization reaction, the η^3-allyl ligand has to rotate in such a way where the C_1 carbon and the hydride should be close at the same side. We tried to locate the transition state for the η^3-allyl ligand rotation, but failed. Only the conformer **6b** was obtained. From **6a**, the shift of H_1 to C_1 atom occurs easily through the transition state **TS(6b/1-(2 t-C$_4$H$_8$))** with very low barrier of 2.49 kcal/mol, and leads to the *trans*-2-butene-coordinated complex **1-(2 t-C$_4$H$_8$)**. In **1-(2 t-C$_4$H$_8$)**, the *trans*-2-butene is stabilized by the Fe···H–C agostic interaction in the vacant axis site and the Fe···HC distance is 1.857 Å. The *trans*-2-butene coordinated complex **1-(2 t-C$_4$H$_8$)** is less stable than ^{OS}**1-(1-C$_4$H$_8$)** by 16.28 [27.30] kcal/mol. We found that the release of *trans*-C_4H_8 from **1-(2 t-C$_4$H$_8$)** is only exoergic by 3.14 kcal/mol and the whole 1-butene isomerization is an endergonic process (Fig. 5).

Fortunately, we obtained all the stationary points along the open-shell singlet path (Fig. 5). From ^{OS}**1-(1-C$_4$H$_8$)**, the H-shift transition state ^{OS}**TS(1-(1-C$_4$H$_8$)/6a)** is slightly more stable by 1.03 [5.07] kcal/mol than **TS(1-(1-C$_4$H$_8$)/6a)**. The first H-shift barrier is 18.21 [29.23] kcal/mol, higher than that (8.7 kcal/mol) catalyzed by $Fe(CO)_3$ fragment [79]. The hydrogen transfer from Fe to the terminal carbon takes place via the open-shell singlet transition state ^{OS}**TS(6b/1-(2 t-C$_4$H$_8$))** with barrier of 1.72 kcal/mol. Especially, the open-shell singlet adduct ^{OS}**1-(2 t-C$_4$H$_8$)** is more stable than the closed-shell singlet **1-(2 t-C$_4$H$_8$)** by 15.41 [19.58] kcal/mol. The isomerization of **1-(1-C$_4$H$_8$)** to **1-(2 t-C$_4$H$_8$)** should be accomplished with C_4H_8 entering. One C_4H_8 molecule coordinates to Fe and *trans*-C_4H_8 releases with an exergonic energy of 19.25 kcal/

mol. The open-shell singlet state path is more favorable thermodynamically and the closed-shell singlet mechanism can be ruled out. This is different from the fact that the closed singlet alkene-coordinated iron complex $Fe(CO)_3(\eta^2$–1-hexene) favors the alkene isomerization [79].

For the triplet state pathway, unfortunately, the crucial H-shift transition state could not be located by our much effort. This is not surprising because the C=C double in ^{3}**1-(1-C$_4$H$_8$)** (Fig. 4) is nearly in the distorted square planar plane and the methylene -CH_2- in C_4H_8 is very far from the Fe center and not available for C-H bond activation and subsequent isomerization. The following triplet stationary points have been located and they are much less stable than the singlets (Fig. S8). Thus, the triplet mechanism for alkene isomerization can be ruled out.

Having ^{OS}**1-(2 t-C$_4$H$_8$)** in hand, we computed the following hydrogenation steps. Starting from ^{OS}**1-(2 t-C$_4$H$_8$)**, one H_2 coordination in η^2 fashion affords the dihydrogen complex $(C_4H_8)[Fe](\eta^2\text{-}H_2)$ ^{OS}**7** (Fig. 6). The formation of ^{OS}**7** is endergonic by 14.99 [26.01] kcal/mol; indicating that H_2 coordination is not favorable thermodynamically. As in case of ^{OS}**TS(2a/3a)**, we found a concerted open-shell singlet transition state for H_2 breaking and C-H formation via the transition state ^{OS}**TS(7/8)** for the formation of hydride and 2-butyl complex **8**. Along the triplet state surface (Fig. S10), the transition state ^{3}**TS(7/8)** for the hydrogen shift in the H-H cleavage process and intermediate ^{3}**8** are much higher in energy than the singlets. The final reductive elimination with the formation of butane from **8** has almost no barrier and is exergonic. It is worth noting that the energy of the open-shell singlet transition state ^{OS}**TS(9/10)** is lower than that of **TS(9/10)** and ^{3}**TS(9/10)** by 6.06 and 1.92 kcal/mol, respectively. As shown in Fig. S10, the triplet intermediates involved in the C-H reductive elimination lie below the closed- and open-shell singlet states. This indicates that the spin crossing might take place from **8** to ^{3}**9** due to the spin-orbit coupling and the triplet mechanism is in competition with the open-shell singlet mechanism in the C-H reductive elimination. On the potential energy surface, the first step of H_2 coordination and insertion is unfavorable due to the higher barrier of 18.21 [25.19] kcal/mol (11.53 [20.40] kcal/mol in the direct hydrogenation of alkene) relative to ^{OS}**1-(1-C$_4$H$_8$)**. Therefore, the reaction path of 1-butene coordination and hydrogenation is more favorable kinetically.

On the basis of our computations, we wish to propose a simplified reaction mechanism of alkene hydrogenation by using bis(imino)pyridine iron dinitrogen complex (^{iPr}PDI)Fe$(N_2)_2$ under one atmosphere of H_2 (Scheme 3). Due to the low thermodynamic stability of the parent complex, the initial step is the N_2 dissociation, which generates intermediate (^{iPr}PDI)Fe(N_2). In the catalytic cycle, the first step should be the replacement of N_2 by alkene to form the active species (^{iPr}PDI)Fe(1-C_4H_8). The next step is H_2 coordination to form (^{Me}PDI)Fe(H_2)(1-C_4H_8). Subsequently, alkene hydrogenation undergoes a concerted open-shell singlet transition of H_2 dissociation and C-H bond formation as well as C=C bond elongation, which results in the formation of the alkyl complex. The last step is the reductive elimination of the formed alkane. In the whole alkene hydrogenation, the open-shell singlet state reaction path is viable, and the H-H bond cleavage is the rate-determining step with barrier of 11.53 [20.40] kcal/mol. Our proposal differs from the mechanism of Chirik et al., where H_2 coordination is oxidative with the formation of dihydride alkene complex. Our results also show that the proposed alkene coordination and isomerization followed by H_2 oxidative addition is not favorable due to the high effective barrier.

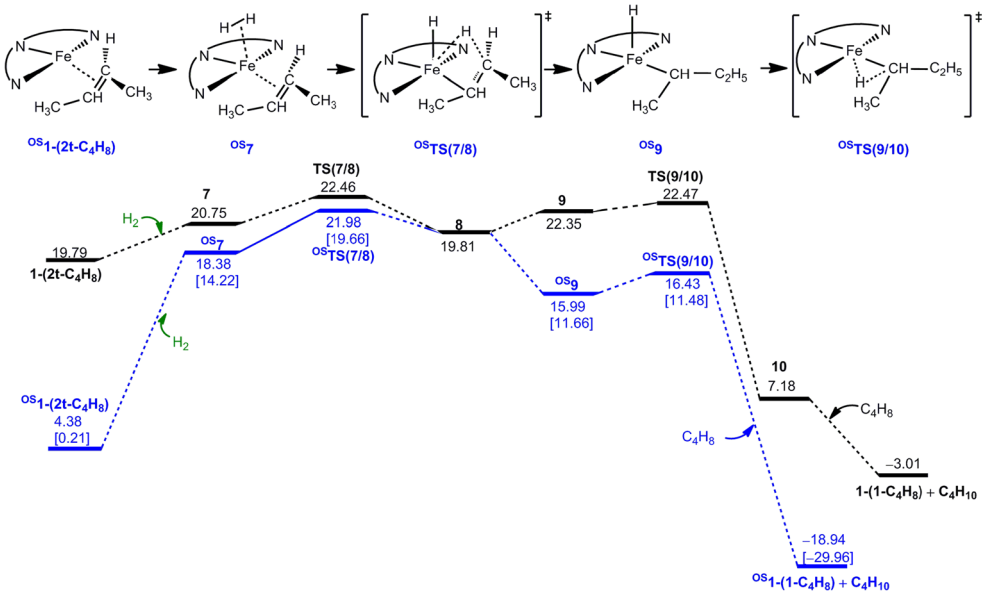

Fig. 6 Free energy profiles (ΔG, kcal/mol) for 2-*trans*-butene hydrogenation (the *black line* is for closed-shell singlet; the *blue line* is for open-shell singlet). The Yamaguchi correction for the open-shell singlet species is given in *square brackets*

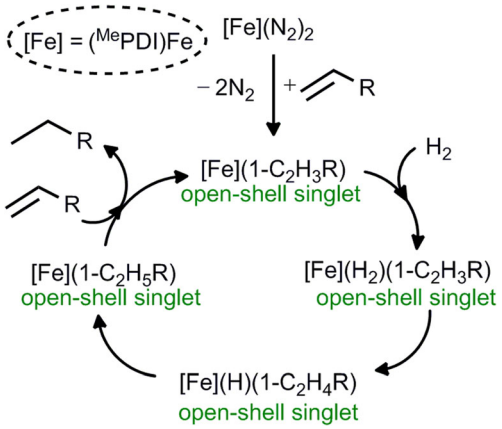

Scheme 3 Simplified catalytic cycle for alkene hydrogenation by bis(imino)pyridine-iron catalysts

Conclusions

We performed UB3LYP density functional theory computation to elucidate the mechanism for alkene hydrogenation catalyzed by bis(imino)pyridine iron dinitrogen complex (^{iPr}PDI)Fe(N_2)$_2$, where the solvation effect of toluene and dispersion effect were included. We found several very interesting points regarding the catalysis steps; different spin states are shown to take place and crossover of several paths is not possible. The redox-active pyridine(diimine)-chelate iron complex shows the characteristic feature of the cooperative electron flow with the ligand and the iron metal in alkene hydrogenation.

(a) The bis(imino)pyridine iron dinitrogen complex, (^{iPr}PDI)Fe(N_2)$_2$, is unstable toward N_2 dissociation and the unsaturated complex, (^{iPr}PDI)Fe(N_2), favors open-shell singlet ground state, which is in close energy with the triplet state, while the corresponding closed singlet state is unstable and high in energy.

(b) The dihydrogen complex (^{iPr}PDI)Fe(H_2) favors triplet state ground state (however, the open-shell singlet is the ground state after Yamaguchi correction); and the dihydride complex from H_2 oxidative addition is unstable and high in energy.

(c) The formation of the dihydrogen (^{iPr}PDI)Fe(H_2) complex is more endergonic than that of 1-butene complex (^{iPr}PDI)Fe(1-C_4H_8) in the open-shell singlet state. This is in agreement with the proposal in literature.

(d) Starting from (^{iPr}PDI)Fe(H_2)(1-C_4H_8), 1-butene hydrogenation takes place via a concerted open-shell singlet transition state involving H-H dissociation, C-H bond formation and C=C double bond elongation. This reaction path is kinetically much more favorable than the alternative reaction path following 1-butene isomerization and H_2 coordination as well as hydrogenation. From **1-(1-C_4H_8)** the open-shell singlet path is generally low in free energy to become a more viable reaction channel. In the whole alkene hydrogenation, the H-H bond cleavage is the rate-determining step with barrier of 11.53 [20.40] kcal/mol.

Acknowledgements This work was supported by the National Natural Science Foundation of China (Grant Nos. 21203115 and 21373131) and the Research Project Supported by Shanxi Scholarship Council of China (Grant No. 2012-057). We thank Dr. Ling Guo and Dr. Bingqiang Wang for helpful discussions. This work was also supported in part by Computer resources at the National Supercomputing Center in Shenzhen (Shenzhen Cloud Computing Center).

Compliance with ethical standards

Conflict of interest The authors declare no competing financial interests.

References

1. Blaser H-U, Spindler F, Thommen M (2008) The handbook of homogeneous hydrogenation. de Vries JG, Elsevier CJ (eds) Wiley-VCH: Weinheim
2. Cipot J, McDonald R, Stradiotto M (2006) Organometallics 25:29–31
3. Hesp KD, Wechsler D, Cipot J, Myers A, McDonald R, Ferguson MJ, Schatte G, Stradiotto M (2007) Organometallics 26:5430–5437
4. Alvarez A, Maclas R, Bould J, Fabra MJ, Lahoz FJ, Oro LA (2008) J Am Chem Soc 130:11455–11466
5. Chirik PJ (2015) Acc Chem Res 48:1687–1695
6. Li L, Zhao H, Wang R (2015) ACS Catal 5:948–955
7. Osborn JA, Wilkinson G, Young JF (1965) Chem Commun 17
8. Osborn JA, Jardine FH, Young JF, Wilkinson G (1966) J Chem Soc A 1711–1732
9. Schrock RR, Osborn JA (1971) J Am Chem Soc 93:3091–3092
10. Crabtree RH (1979) Acc Chem Res 12:331–337
11. Knowles WS (2002) Angew Chem Int Ed 41:1998–2007
12. Noyori R (2002) Angew Chem Int Ed 41:2008–2022
13. Sperger T, Sanhueza IA, Kalvet I, Schoenebeck F (2015) Chem Rev 115:9532–9586
14. Bolm C, Legros J, Le Paih J, Zani L (2004) Chem Rev 104:6217–6254
15. Bauer I, Knölker H-J (2015) Chem Rev 115:3170–3387
16. Small BL, Brookhart M, Bennett AMA (1998) J Am Chem Soc 120:4049–4050
17. Britovsek GJP, Bruce M, Gibson VC, Kimberley BS, Maddox PJ, Mastroianni S, McTavish SJ, Redshaw C, Solan GA, Strömberg S, White AJP, Williams DJ (1999) J Am Chem Soc 121:8728–8740
18. Knijnenburg Q, Horton AD, van der Heijden H, Kooistra TM, Hetterscheid DGH, Smits JMM, de Bruin B, Budzelaar PHM, Gal AW (2005) J Mol Catal A Chem 232:151–159
19. Bart SC, Lobkovsky E, Chirik PJ (2004) J Am Chem Soc 126:13794–13807
20. Archer AM, Bouwkamp MW, Cortez MP, Lopkovsky E, Chirik PJ (2006) Organometallics 25:4269–4278
21. Bart SC, Lobkovsky E, Bill E, Chirik PJ (2006) J Am Chem Soc 128:5302–5303

22. Trovitch RJ, Lopkovsky E, Bill E, Chirik PJ (2008) Organometallics 27:1470–1478
23. Russell SK, Darmon JM, Lopkovsky E, Chirik PJ (2010) Inorg Chem 49:2782–2792
24. Tondreau AM, Atienza CCH, Weller KJ, Nye SA, Lewis KM, Delis JGP, Chirik PJ (2012) Science 335:567–570
25. Ward MD, McCleverty JA (2002) J Chem Soc Dalton Trans 275
26. Schröder D, Shaik S, Schwarz H (2000) Acc Chem Res 33:139–145
27. Bellows SM, Cundari TR, Holland PL (2013) Organometallics 32: 4741–4751
28. Trovitch RJ, Lobkovsky E, Chirik PJ (2008) J Am Chem Soc 130: 11631–11640
29. Lee CT, Yang WT, Parr RG (1988) Phys Rev B 37:785–789
30. Becke AD (1993) J Chem Phys 98:5648–5652
31. Stephens PJ, Devlin FJ, Chabalowski CF, Frisch MJ (1994) J Phys Chem 98:11623–11627
32. Khoroshun DV, Musaev DG, Vreven T, Morokuma K (2001) Organometallics 20:2007–2026
33. Sharon DA, Mallick D, Wang B, Shaik S (2016) J Am Chem Soc 138:9597–9610
34. Long GT, Weitz E (2000) J Am Chem Soc 122:1431–1442
35. Glascoe EA, Sawyer KR, Shanoski JE, Harris CB (2007) J Phys Chem C 111:8789–8795
36. Hay PJ, Wadt WR (1985) J Chem Phys 82:299–310
37. Hehre WJ, Ditchfield R, Pople JA (1972) J Chem Phys 56:2257–2261
38. Hariharan PC, Pople JA (1973) Theor Chim Acta 28:213–222
39. Gonzalez C, Schlegel HB (1989) J Chem Phys 90:2154–2161
40. Gonzalez C, Schlegel HB (1990) J Phys Chem 94:5523–5527
41. Bachler V, Olbrich G, Neese F, Wieghardt K (2002) Inorg Chem 41: 4179–4193
42. Cheng L, Wang J, Wang M, Wu Z (2009) Dalton Trans 3286–3297
43. Peng D, Zhang Y, Du X, Zhang L, Leng X, Walter MD, Huang Z (2013) J Am Chem Soc 135:19154–19166
44. Reed AE, Weinstock RB, Weinhold F (1985) J Chem Phys 83:735–746
45. Cossi M, Rega N, Scalmani G, Barone V (2003) J Comput Chem 24:669–681
46. Miertus S, Scrocco E, Tomasi J (1981) J Chem Phys 55:117–129
47. Miertus S, Tomasi J (1982) J Chem Phys 65:239–245
48. Grimme S, Antony J, Ehrlich S, Krieg H (2010) J Chem Phys 132: 154104
49. Grimme S, Ehrlich S, Goerigk L (2011) J Comput Chem 32:1456–1465
50. Winget P, Cramer CJ, Truhlar DG (2004) Theor Chem Accounts 112:217–227
51. Seeger R, Pople JA (1977) J Chem Phys 66:3045–3050
52. Bauernschmitt R, Ahlrichs R (1996) J Chem Phys 104:9047–9052
53. Yamaguchi K, Jensen F, Dorigo A, Houk KN (1988) Chem Phys Lett 149:537–542
54. Frisch MJ, Trucks GW, Schlegel HB, Scuseria GE, Robb MA, Cheeseman JR, Scalmani G, Barone V, Mennucci B, Petersson GA, Nakatsuji H, Caricato M, Li X, Hratchian HP, Izmaylov AF, Bloino J, Zheng G, Sonnenberg JL, Hada M, Ehara M, Toyota K, Fukuda R, Hasegawa J, Ishida M, Nakajima T, Honda Y, Kitao O, Nakai H, Vreven T, Montgomery Jr JA, Peralta JE, Ogliaro F, Bearpark M, Heyd JJ, Brothers E, Kudin KN, Staroverov VN, Keith T, Kobayashi R, Normand J, Raghavachari K, Rendell A, Burant JC, Iyengar SS, Tomasi J, Cossi M, Rega N, Millam JM, Klene M, Knox JE, Cross JB, Bakken V, Adamo C, Jaramillo J, Gomperts R, Stratmann RE, Yazyev O, Austin AJ, Camii R, Pomelli C, Ochterski JW, Martin RL, Morokuma K, Zakrzewski VG, Voth GA, Salvador P, Dannenberg JJ, Dapprich S, Daniels AD, Farkas Ö, Foresman JB, Ortiz JV, Cioslowski J, Fox DJ (2013) Gaussian 09, Revision E.01. Gaussian, Inc., Wallingford
55. Stieber SCE, Milsmann C, Hoyt JM, Turner ZR, Finkelstein KD, Wieghardt K, DeBeer S, Chirik PJ (2012) Inorg Chem 51:3770–3785
56. Booth CH, Walter MD, Kazhdan D, Hu Y-J, Lukens WW, Bauer ED, Maron L, Eisenstein O, Andersen RA (2009) J Am Chem Soc 131:6480–6491
57. Smith KM, Poli R, Harvey JN (2000) New J Chem 24:77–80
58. Harvey JN (2004) Faraday Discuss 127:165–177
59. Ganguly G, Malakar T, Paul A (2015) ACS Catal 5:2754–2769
60. Ortuño MA, Cramer CJ (2017) J Phys Chem A 121:5932–5939
61. Trovitch RJ, Lobkovsky E, Chirik RJ (2006) Inorg Chem 45:7252–7260
62. Gorgas N, Alves LG, Stöger B, Martins AM, Veiros LF, Kirchner K (2017) J Am Chem Soc 139:8130–8133
63. Yu RP, Darmon JM, Semproni SP, Turner ZR, Chirik PJ (2017) Organometallics 36:4341–4343
64. Dub PA, Gordon JC (2017) ACS Catal 7:6635–6655
65. Polo V, Al-Saadi AA, Oro LA (2014) Organometallics 33:5156–5163
66. Hoyt JM, Sylvester KT, Semproni SP, Chirkik PJ (2013) J Am Chem Soc 135:4862–4877
67. Tondreau AM, Atienza CCH, Darmon JM, Milsmann C, Hoyt HM, Weller KJ, Nye SA, Lewis KM, Boyer J, Delis JGP, Lobkovsky E, Chirik PJ (2012) Organometallics 31:4886–4893
68. Li L, Lei M, Sakaki S (2017) Organometallics 36:3530–3538
69. Poli R, Harvey JN (2003) Chem Soc Rev 32:1–8
70. Ozawa F, Hikida T, Hayashi T (1994) J Am Chem Soc 116:2844–2849
71. Sakaki S, Mizoe N, Sugimoto M, Musashi Y (1999) Coord Chem Rev 190:933–960
72. Sakaki S, Sumimoto M, Fukuhara M, Sugimoto M, Fujimoto H, Matsuzaki S (2002) Organometallics 21:3788–3802
73. Cheng C, Kim BG, Guironnet D, Brookhart M, Guan CJ, Wang DY, Krogh-Jespersen K, Goldman AS (2014) J Am Chem Soc 136: 6672–6683
74. Tao JC, Sun FS, Fang T (2012) J Org Chem 698:1–6
75. Harrod JF, Chalk AJ (1964) J Am Chem Soc 86:1776–1779
76. Harrod JF, Chalk AJ (1966) J Am Chem Soc 88:3491–3497
77. Davies NR (1964) Nature 201:490–491
78. Davies NR (1964) Aust J Chem 17:212–218
79. Sawyer KR, Glascoe EA, Cahoon JF, Schlegel JP, Harris CB (2008) Organometallics 27:4370–4379